Comparison of ADCP and ECCOv4r4 Currents in the Pacific Equatorial Undercurrent

DAVID HALPERN,[a] MEGAN K. LE,[b,c] TIMOTHY A. SMITH,[d,e,f] AND PATRICK HEIMBACH[d,g,h]

[a] *Scripps Institution of Oceanography, University of California, San Diego, La Jolla, California*
[b] *Department of Computer Science, The University of Texas at Austin, Austin, Texas*
[c] *Department of Mathematics, The University of Texas at Austin, Austin, Texas*
[d] *Oden Institute for Computational Engineering and Sciences, The University of Texas at Austin, Austin, Texas*
[e] *Cooperative Institute for Research in Environmental Sciences, Boulder, Colorado*
[f] *Physical Sciences Laboratory, National Oceanic and Atmospheric Administration, Boulder, Colorado*
[g] *Jackson School of Geosciences, The University of Texas at Austin, Austin, Texas*
[h] *Institute for Geophysics, The University of Texas at Austin, Austin, Texas*

(Manuscript received 2 February 2023, in final form 10 August 2023, accepted 9 October 2023)

ABSTRACT: The Pacific Equatorial Undercurrent (EUC) flows eastward across the Pacific at the equator in the thermocline. Its variability is related to El Niño. Moored acoustic Doppler current profiler (ADCP) measurements recorded at four widely separated sites along the equator in the EUC were compared to currents generated by version 4 release 4 of the Estimating the Circulation and Climate of the Ocean (ECCOv4r4) global model–data synthesis product. We are interested to learn how well ECCOv4r4 currents could complement sparse in situ current measurements. ADCP measurements were not assimilated in ECCOv4r4. Comparisons occurred at 5-m depth intervals at 165°E, 170°W, 140°W, and 110°W over time intervals of 10–14 years from 1995 to 2010. Hourly values of ECCOv4r4 and ADCP EUC core speeds were strongly correlated, similar for the EUC transport per unit width (TPUW). Correlations were substantially weaker at 110°W. Although we expected means and standard deviations of ECCOv4r4 currents to be smaller than ADCP values because of ECCOv4r4's grid representation error, the large differences were unforeseen. The appearance of ECCOv4r4 diurnal-period current oscillations was surprising. As the EUC moved eastward from 170° to 140°W, the ECCOv4r4 TPUW exhibited a much smaller increase compared to the ADCP TPUW. A consequence of smaller ECCOv4r4 EUC core speeds was significantly fewer instances of gradient Richardson number (Ri) less than 1/4 above and below the depth of the core speed compared to Ri computed with ADCP observations. We present linear regression analyses to use monthly-mean ECCOv4r4 EUC core speeds and TPUWs as proxies for ADCP measurements.

SIGNIFICANCE STATEMENT: Hundreds of scientific papers have used ECCO data products generated with a continually evolving state-of-the-art ocean-model–data synthesis system. We ask, How representative is the latest version of ECCO equatorial ocean currents? We use independent in situ current measurements as the reference dataset to establish the accuracy of ECCO currents in the tropical Pacific. Attention is focused on the Pacific Equatorial Undercurrent (EUC) because it contributes to the formation of El Niño and La Niña events. ECCO EUC core speeds were smaller in magnitude and less variable in time compared to observations. As a consequence, ECCO currents generated smaller vertical mixing in the EUC compared to that inferred from current measurements. We developed a linear regression model to improve representation of monthly-mean ECCO currents.

KEYWORDS: Tropics; El Niño; Model evaluation/performance; Ocean models; Reanalysis data

1. Introduction

Since the 1960s development of the Ocean General Circulation Model (OGCM), the OGCM has become an extremely valuable instrument to study four-dimensional structures of global ocean currents. Constraining an OGCM with in situ and satellite measurements of ocean surface topography, salinity, temperature, and other variables improved the representativeness of OGCM-generated currents. However, no OGCM combined with data assimilation, named model–data synthesis, produced perfect currents because of OGCM representation errors, observation errors, data assimilation errors, and errors in parameterizing subgrid-size processes.

In 1999, the Estimating the Circulation and Climate of the Ocean (ECCO) Consortium established a four-dimensional variational data assimilation system with the Massachusetts Institute of Technology General Circulation Model (MITgcm) (Marshall et al. 1997a,b) to routinely produce a hindcast or state estimate (akin to a reanalysis, but different in important ways such as elimination of data assimilation disturbance) of oceanographic conditions (Stammer et al. 2002). ECCO solutions are advantageous because they (i) do not contain discontinuities

Denotes content that is immediately available upon publication as open access.

Le's current affiliation: Department of Electrical Engineering and Computer Science, Massachusetts Institute of Technology, Cambridge, Massachusetts.

Corresponding author: David Halpern, dhalpern@ucsd.edu

DOI: 10.1175/JTECH-D-23-0013.1

when and where data are ingested and (ii) satisfy OGCM conservation laws of heat, salt, and momentum for the complete assimilation period (Wunsch and Heimbach 2013; Stammer et al. 2016). Over the years, ECCO Consortium et al. (2021) consistently improved the OGCM–data system with (i) advancements to the OGCM, (ii) enhancements to the data assimilation scheme, (iii) assimilation of additional in situ and satellite observations, (iv) improvements in the data and prior uncertainty estimates, and (v) extension of the estimation period to cover the years 1992–2017. The latest version as of this writing is named ECCO version 4 release 4 (ECCOv4r4; ECCO Consortium 2021).

We are interested to learn how well ECCOv4r4 currents could supplement sparse measurements of in situ currents of the Pacific Equatorial Undercurrent (EUC). The approximately 100-m-thick EUC, discovered in 1952 (Cromwell et al. 1954), flows eastward across the Pacific at the equator in the thermocline at depths ranging from 200 m in the west to 50 m in the east (Philander 1990). The EUC is confined to the narrow equatorial zone centered at the equator where transport is maximum and decreases poleward becoming zero, more or less, at 1.5°S and 1.5°N (Philander 1990). Maximum speeds within the EUC reach 200 cm s^{-1} (Halpern 1987a). The EUC's north–south narrowness with strong meridional gradients of zonal current north and south of the equator and thin layers of intense vertical gradients of zonal current above and below the depth of maximum speed present challenges for numerical circulation models with north–south and vertical grid dimensions of tens of kilometers and many meters, respectively, to adequately represent in situ current measurements at a specific location, such as 100-m depth and 0° latitude.

The location of the EUC at the equator means the EUC is not in geostrophic balance because the Coriolis force is zero at the equator. Thus, salinity and temperature measurements are not practical to observe the EUC, and direct current measurements are required to monitor the EUC. In the mid-1970s, Halpern (2021) developed moored-buoy technology to record long time series of upper-ocean currents and temperature at the equator where water depths are 4–5 km. His pioneering methodology produced the first observation of a Kelvin wave propagating eastward within the EUC (Knox and Halpern 1982) to confirm many aspects of theories of equatorial Kelvin waves, the first estimate of vertical velocity within and above the EUC computed from the continuity equation (Halpern and Freitag 1987), and the first observation of the time evolution of the disappearance of the EUC in the eastern Pacific in a strong El Niño event (Halpern 1987a).

In the climatological-mean coupled ocean–atmosphere Walker circulation along the equator, sea surface temperature (SST) is about 5°C lower in the eastern equatorial Pacific, e.g., at the Galapagos Archipelago at about 90°W, compared to SST west of the date line. Along the equator surface wind blows westward (i.e., easterly trade wind) from higher barometric pressure toward lower barometric pressure, thermocline slopes upward from west to east, surface waters flow westward in the South Equatorial Current, and the EUC completes the zonal circulation in the upper ocean. As the EUC flows eastward in the thermocline, water is entrained into it from the Northern and Southern Hemispheres, and EUC waters are exported vertically (Philander 1990), where, in the eastern Pacific, upwelling influences SST.

The El Niño and La Niña phenomenon represents a quasi-oscillatory 5–7-yr period increase and decrease, respectively, of SST in the eastern equatorial Pacific. Bjerknes (1969) and Rowntree (1972) showed how the occurrence of an El Niño event would influence atmospheric circulation in middle latitudes, which were the first indications of the global impact of interannual SST variations in the eastern equatorial Pacific (i.e., an El Niño event). Bjerknes (1969) noted that the EUC, through its vertical displacements, had an important connection to the onset, maintenance, and dissipation of an El Niño event.

Aware of the substantial global economic impact caused by the El Niño event in 1982/83 [see Callahan and Mankin (2023) for the latest estimate of $4.1 trillion] and of mid-1970s ocean current measuring technology developments (Halpern 2021), the World Climate Research Program (1985) recommended continuous in situ current measurements of the EUC throughout the 1985–94 Tropical Ocean and Global Atmosphere (TOGA) program. When the TOGA program ended, in situ measurements of currents and other variables were continued while plans were made to sustain the El Niño monitoring system that had been developed under the auspices of the TOGA program. In 1997, the U.S. extensive array of moored meteorological and oceanographic observations in the tropical Pacific, including current measurements in the EUC, were operationalized (https://tao.ndbc.noaa.gov/proj_overview/taohis_ndbc.shtml) to sustain observations to improve understanding of the dynamics of El Niño and La Niña events and to evaluate model representations of El Niño and La Niña events [see Philander and Siegel (1985) for the first such evaluation]. The incorrect forecast of a major El Niño event in 2014 (Plumer 2014), the influence of El Niño on global warming (Joshi 2023), and the effect of El Niño on global economic growth (Callahan and Mankin 2023) maintain attention on the El Niño phenomenon and, consequently, on the EUC. It is noteworthy that the Tropical Pacific Observing System 2020 (TPOS2020) project (Kessler et al. 2021) proposes to expand locations and vertical resolution of direct current measurements in the EUC, indicating continued monitoring of the EUC that had begun in 1977. However, the TPOS2020 project expects to have four 30°-longitude regions along the equator without in situ upper-ocean current measurements, providing the need for model-generated currents.

In an overview of the paper, we began with a description of oceanographic conditions in the narrow equatorial zone and an explanation of how large-scale ocean–atmosphere interactions produce the EUC, the El Niño and La Niña phenomena, and their connections. Then, we explain the acquisition and characteristics of ADCP and ECCOv4r4 currents. This is followed by quantitative evaluations of similarities and differences of vertical distributions of record-length time-averaged current components. We believe the following aspects of our

comparative study between model-generated currents and observed currents have not appeared in the literature for any location throughout the equatorial ocean and perhaps in the global ocean. A linear regression model relating ADCP and ECCOv4r4 core speeds is presented. Because it is extremely rare for time series observations of EUC transport to occur, we examine the correspondence between ADCP and ECCOv4r4 transports per unit width at the equator. Time variations of ADCP and ECCOv4r4 current components were examined with the standard deviation computed at all depths and all sites and with a very small number of spectra. Spectra serendipitously revealed a surprising result. The vertical shear represented by the gradient Richardson number is evaluated. Finally, numerous findings are summarized in a list. Concluding remarks with suggestions for further research completes the report.

2. Methodology

The time origin of ECCOv4r4 data products coincided with the August 1992 launch of the Topography Experiment/Poseidon ocean surface topography satellite mission (https://www.jpl.nasa.gov/missions/topex-poseidon). Since that time, ADCP measurements in the Pacific EUC were acquired at 0°, 165°E and 0°, 170°W by the National Oceanic and Atmospheric Administration (NOAA) Pacific Marine Environmental Laboratory (PMEL) (https://www.pmel.noaa.gov/gtmba/pmel-theme/pacific-ocean-tao). The 0° latitude associated with ADCP measurements recorded on the equator will not be mentioned hereafter, e.g., the coordinates of the ADCP measurements at 0°, 140°W will be designated 140°W. No off-equatorial ADCP measurements were recorded. The ADCP measurements at 140° and 110°W began in the mid-1990s. In the early 2000s, the NOAA National Data Buoy Center (NDBC) partnered with the PMEL to record the ADCP measurements (https://tao.ndbc.noaa.gov/proj_overview/qc_ndbc.shtml#adcp).

ECCOv4r4 did not assimilate ADCP measurements at 165°E, 170°W, 140°W, and 110°W or other in situ current measurements recorded along and near the equator. We thus consider these ADCP measurements to be independent ground truth for evaluating ECCOv4r4 currents. The ADCP currents had considerably less uncertainty [as noted in section 2b(2)].

The 165°E, 170°W, 140°W, and 110°W locations selected for the comparative study encompassed a variety of oceanographic conditions (Philander 1990). Halpern et al. (2022) showed these moored-buoy positions superimposed on the Colin et al. (1971) equatorial longitude–depth section of upper-ocean temperatures. While the EUC thickness was about 100 m at each site, the depth of the EUC core speed increased toward the west and was more than 150 m deeper at 165°E than at 110°W. Near-surface mixed layer thicknesses increased westward from less than 25 m at 110°W to about 100 m at 165°E. Thermocline intensity, as measured by the vertical gradient of temperature between the 15° and 25°C isotherms, was essentially the same between 170° and 110°W and slightly weaker at 165°E.

a. ADCP currents

An upward-looking, narrowband, four-acoustic-beam Teledyne RD Instrument (RDI) ADCP was located at a nominal depth of about 250–300 m at the top of an NDBC and PMEL subsurface mooring at each of the four sites, where the water depth was 4–5 km. The RDI ADCP transmitted a 150-kHz acoustic pulse, measured the Doppler shift in the backscattered acoustic energy, and acquired data in 8.68-m bins with a 3-s sampling rate. External data processing yielded vertical profiles of 15-min-averaged zonal and meridional velocities over 5-m-thick layers (Plimpton et al. 2004; Teledyne RD Instruments 2011; https://www.pmel.noaa.gov/gtmba/pmel-theme/pacific-ocean-tao). In the Pacific EUC, mean current speeds and directions recorded with an RDI ADCP differed by 5 cm s^{-1} and 2.5°, respectively, from those recorded with fixed-level vector-averaging current meters (VACMs) and vector-measuring current meters (VMCMs) (Plimpton et al. 2004). The VMCM (Weller and Davis 1980) is considered the gold standard in moored current measurements in the EUC and the VACM is an excellent approximation of it (Halpern 1987b). Coincident current measurements recorded with fixed-level VACMs and VMCMs did not produce adjustments to the ADCP measurements (https://tao.ndbc.noaa.gov/proj_overview/qc_ndbc.shtml#adcp).

Mooring motions produced downward displacements of the ADCP which were generally less than 80 m and rarely greater than 100 m (Plimpton et al. 2004). The PMEL and NDBC data processing systems accounted for the variable depths of ADCP data with in situ measurements of pressure (i.e., subsurface depth), temperature, and salinity (Plimpton et al. 2004).

We selected record lengths at 165°E, 170°W, 140°W, and 110°W of 1996–2007, 1995–2005, 1997–2010, and 1996–2005, respectively. Each time interval began 1 January and ended 31 December. Each record length satisfied criteria of maximum time interval, minimum number of gaps, and minimum total time of gaps. Each time interval encompassed the very strong El Niño event of May 1997–May 1998 when the EUC disappeared and was replaced by the westward-flowing South Equatorial Current (SEC). One-hour-averaged ADCP measurements at 5-m depth intervals were extracted from the PMEL at https://www.pmel.noaa.gov/gtmba/pmel-theme/pacific-ocean-tao.

The ADCP data were not continuous with depth and time because of near-surface bubbles, water clarity, sidelobe interference at the sea surface, instrument malfunctions, and deployment continuity issues. The ADCP data were analyzed at the following depth intervals: 40–260 m at 165°E, 40–260 m at 170°W, 40–235 m at 140°W, and 35–195 m at 110°W. In the selected depth interval at each site, the ADCP measurements at depths at and near the depth of the EUC core speed had about 99% of the maximum number of data values; i.e., there were not many data gaps. For example, at 140°W at 75-m depth (Fig. 1), which was 30 m above the depth of the core speed, the record length was 14 years, the number of 1-h-averaged ADCP measurements was 122 389, the total number of gaps was 66, the total time interval of gaps was 324 h, only 2 gaps were longer than 12 h, and the maximum gap time was 31 h.

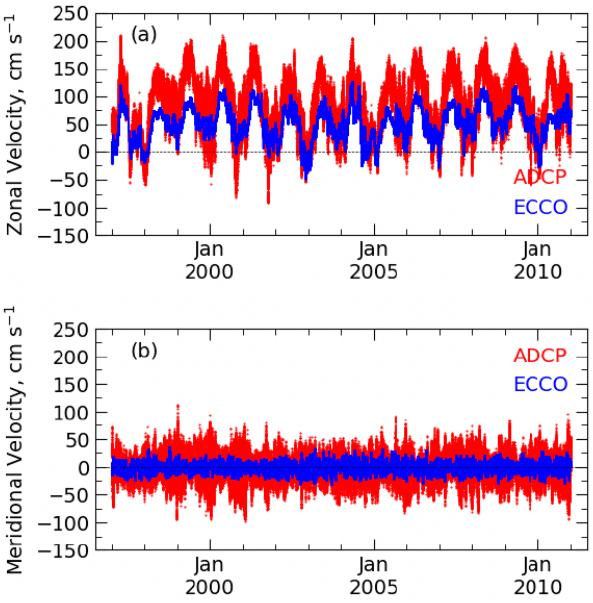

FIG. 1. Time series of 1-h-averaged (a) east–west and (b) north–south currents produced by ECCOv4r4 (blue) and measured with the ADCP (red) during 1 Jan 1997–31 Dec 2010 at 75-m depth at 140°W. Eastward and northward motions are positive values and westward and southward motions are negative values.

b. *ECCOv4r4 currents*

Smith (2021) reran the ECCOv4r4 Central Production architecture (ECCO Consortium et al. 2021) to extract meridional and zonal currents at the model time step of 1 h.

In ECCOv4r4, there is a latitudinal grid boundary at the equator and adjacent latitudinal grid boundaries at 0.4°S and 0.4°N. The north–south dimension of grid cells increased gradually to 1° at 10°N and 10°S, where the dimension then decreased poleward in accordance with isotropic grid scaling (Forget et al. 2015). The north–south grid boundary was an integer-numbered meridian, e.g., 140°W; i.e., the resolution in zonal direction was nominally 1°. The finite-volume formulation of MITgcm means that the modeled velocities represent an average across the boundary of a cell whereas ADCPs are point measurements. For example, the zonal current at 0°, 140°W was equal to the average of zonal currents from 0.4°S to 0.0° and from 0.0° to 0.4°N along 140°W. The meridional current at 0°, 140°W was equal to the average of meridional currents along 0° from 141° to 140°W and from 140° to 139°W. Thus, ECCOv4r4 zonal and meridional currents at each mooring represented north–south and east–west distances of 88.8 and 222 km, respectively. Thus, we expected a priori that ECCOv4r4 zonal current speeds would be smaller than ADCP measurements at the equator because of the OGCM's representation error (Fukumori 2006; Janjić et al. 2017). ECCOv4r4's relatively large north–south grid dimension failed to capture the EUC north–south gradient of zonal current, which yielded diminished ECCOv4r4 EUC core speeds compared to ADCP observations at the equator. Karnauskas et al. (2020) noted a decrease of EUC core speed at the equator with increasing climate model meridional grid dimensions, with a north–south spacing of 0.25° yielding more representative core speeds compared to a 0.33°-grid size and much more accurate compared to 0.5° and 1.0° dimensions; a 2° meridional grid size produced unrepresentative small EUC core speeds.

Additional characteristics of ECCOv4r4 currents limiting their agreement with in situ current measurements include imprecise parameterizations of vertical mixing, horizontal mixing, and air–sea interactions, neglect of physical processes such as tides, imperfect data assimilation schemes, and inadequate representation of the observations within the data assimilation system. The EUC is primarily wind driven and the type of atmospheric forcing, especially the easterly surface wind stress along the equator (Philander 1990), will influence the EUC produced by ECCOv4r4. Prevailing southerly wind stress has the potential to shift the position of the EUC slightly southward of the equator (Philander 1973; Gill 1975). Off-equatorial currents are driven by curl of surface wind stress (Sverdrup 1947). Ou et al. (2020) state that the European Centre for Medium-Range Weather Forecasts (ECMWF) interim reanalysis (ERA-Interim), which was superseded by ERA5 on 31 August 2019, provided ECCOv4r4 atmospheric forcing. ERA5 wind stress components were interpolated on the ECCOv4r4 grid at 6-h intervals (Ou et al. 2020). These wind stress fields served as first guess (along with other surface atmospheric fields) in ECCOv4's inverse modeling scheme. These fields were adjusted (i.e., inverted for) as part of the gradient-based minimization of the model–data misfit function. The adjoint model computes the gradient of the misfit function with respect to the surface forcing.

Along the vertical direction above 400-m depth, which is defined as the lowermost depth of the EUC, the thicknesses of 21 vertical levels of ECCOv4r4 were 2–10 times larger than the uniform 5-m thickness of ADCP levels. Higher resolution (i.e., smaller grid dimension) would improve the representation of ECCOv4r4 currents, especially near the depth of the maximum eastward speed. Unequaled depths of ECCOv4r4 and ADCP currents were harmonized by linearly interpolating ECCOv4r4 currents to 5-m depth intervals.

To synchronize joint analyses of ADCP and ECCOv4r4 data, artificial data gaps were created in ECCOv4r4 currents by subsetting ECCOv4r4 data to match ADCP data gaps.

3. Results

a. *Overview*

Figure 1 illustrates the potential richness of a comparative study of ECCOv4r4 and ADCP currents in the Pacific EUC. The specific location chosen for Fig. 1, 75-m depth and 140°W, was known to have strong meridional and zonal currents (Halpern et al. 1988). Notable features are as follows: 1) ECCOv4r4 meridional and zonal current speeds were considerably smaller than those measured with an ADCP, 2) ECCOv4r4 and ADCP zonal currents were highly correlated (correlation coefficient of 0.82), and 3) only a meager 14% of the ECCOv4r4 and ADCP meridional current variances were linearly related. A correlation coefficient greater than 0.71 is

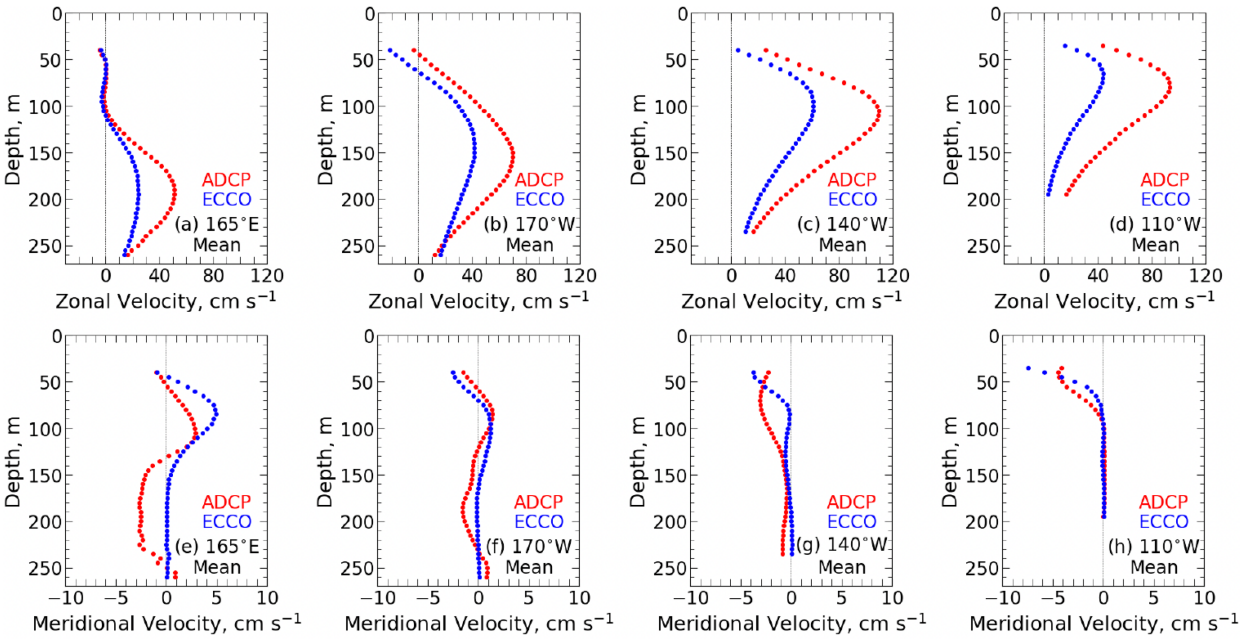

FIG. 2. Vertical profiles of record-length mean (top) zonal and (bottom) meridional currents at (a),(e) 165°E, (b),(f) 170°W, (c),(g) 140°W, and (d),(h) 110°W along the equator. Blue and red curves represent ECCOv4r4 and ADCP, respectively.

considered high (low) because more (less) than 50% of the variances of both datasets were linearly related. The annual cycle dominated zonal currents with ECCOv4r4 solutions having a smaller amplitude than ADCP observations (Fig. 1a); no major time scale was visible in meridional currents (Fig. 1b). The ECCOv4r4 zonal current mean, variance, maximum, and minimum values were 36%, 67%, 40%, and 48% smaller, respectively, than ADCP measurements. The ADCP zonal currents had much larger temporal fluctuations compared to ECCOv4r4 currents, which produced a substantial root-mean-square (rms) difference of 44.2 cm s^{-1}. The rms difference of ECCOv4r4 and ADCP meridional currents was 21.7 cm s^{-1} and more than 7 times greater than the ADCP or ECCOv4r4 mean. The ECCOv4r4 meridional current mean, variance, maximum, and minimum values were 87%, 85%, 69%, and 68% smaller than ADCP data, respectively.

The comparison illustrated in Fig. 1 was not an outlier. It was representative of the ADCP and ECCOv4r4 datasets in the high-speed region of the EUC at the four sites. Our comparative study will explore spatial variations of tens of meters with depth and tens of degrees in longitude of ECCOv4r4 and ADCP current differences over time scales ranging from hours to years.

b. *Mean currents*

At each site, the depth distributions of ECCO4r4 and ADCP mean zonal currents had excellent qualitative agreement with the classical profile of the EUC (Figs. 2a–d). However, quantitative differences were substantial. Throughout the four sites, the 5-m-thick ECCOv4r4 mean eastward current was less than that measured with the ADCP (Figs. 2a–d), except for three depths near the bottom of the EUC at 170°W (Fig. 2b). The depth- and four-site-averaged ECCOv4r4 eastward current was 24.1 cm s^{-1} or 48% smaller than the corresponding ADCP zonal current. The four-site average depth of maximum mean ECCOv4r4 eastward current was 7 m less than ADCP, illustrating excellent correspondence between the ECCOv4r4 and ADCP depths of the EUC core speed. Section 3c describes features of maximum eastward currents.

The depth and four-site-averaged ECCOv4r4 and ADCP mean meridional currents were 0.0 and −3.7 cm s^{-1}, respectively (Figs. 2d–g). The difference was smaller than the 5 cm s^{-1} accuracy of moored ADCP current measurements in the EUC to be considered significant.

c. *EUC core speed*

The EUC core speed is defined as the maximum eastward speed. At several sites, the vertical gradient of the zonal current at depths near the depth of the core speed was very small with equivalent ADCP maximum mean eastward current, to within 1 cm s^{-1}, at two to three adjacent depths (Figs. 2a–d). The EUC core-speed depth was chosen to minimize the difference between ADCP and ECCOv4r4 record-length mean values. Depths of EUC core speeds were 190, 155, 105, and 75 m at 165°E, 170°W, 140° and 110°W, respectively.

Figure 3 displays time series of ECCOv4r4 and ADCP core speeds at each site. Dominant fluctuations are visible at the annual period, season to interannual times (e.g., in November 1997–January 1998 during an El Niño event), and at submonthly time scales. The four-site-averaged ECCOv4r4 and ADCP mean core speeds were 42.3 and 80.9 cm s^{-1}, respectively. The average ECCOv4r4 core speed was a substantial 48% smaller than ADCP. The sizable 38.6 cm s^{-1} difference was a defining feature of the intercomparison test. Compared

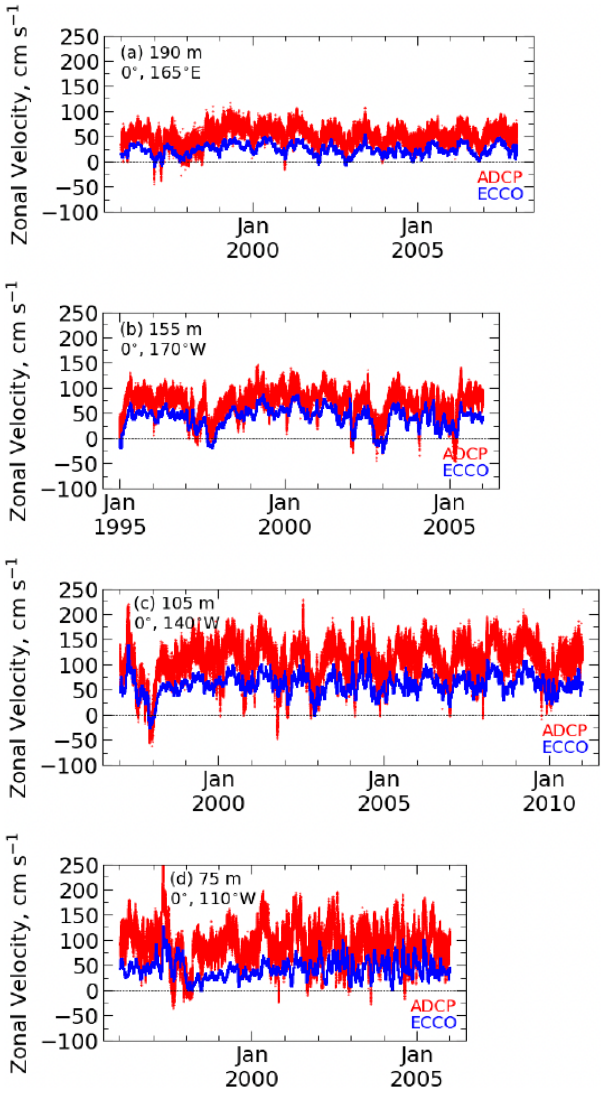

FIG. 3. Time series of 1-h-averaged ECCOv4r4 (blue curve) and ADCP (red curve) EUC eastward speeds at the depth of the record-length mean maximum eastward speed at (a) 190 m at 0°, 165°E; (b) 155 m at 0°, 170°W; (c) 105 m at 0°, 140°W; and (d) 75 m at 0°, 110°W.

to ADCP measurements at the equator where the EUC core speed was maximum, the ECCOv4r4 produced a core speed representative of a considerable north–south distance poleward from the equator (section 2b). The Johnson et al. (2002) irregularly sampled decadal-mean measurements indicated that the core speed at 0.4°N, 140°W would be about 20% lower compared to its value at the equator. Assuming a linear decrease in core speed with latitude from the equator, the average ECCOv4r4 core speed along 140°W between 0° and 0.4°N would be expected to be about 10% lower than at the equator. This quantity is too small to account for the 48% difference between ECCOv4r4 and ADCP core speeds.

Considerably larger core speeds occurred at 140° and 110°W compared to 165°E and 170°W (Fig. 3). The ECCOv4r4 solutions of 1-h-averaged peak current speeds rarely reached 100 cm s^{-1}. However, on several occasions the ADCP recorded peak current speeds greater than 200 cm s^{-1}, which were first observed with multiple fixed-level current measurements recorded beneath a surface float tautly moored to the ocean bottom at 0°, 125°W in 1977 (Halpern 2021).

Mean longitudinal gradients of ECCOv4r4 core speeds from 165°E to 170°W, 170° to 140°W, and 140° to 110°W were 0.68. 0.67, and −0.60 cm s^{-1} per degree longitude, respectively. Corresponding values for ADCP core speeds were 0.76, 1.30, and −0.53 cm s^{-1} per degree longitude, respectively. From 170° to 140°W the ECCOv4r4 core speed increased only half as much as ADCP observations. It is tempting to suppose that this feature was related to ECCOv4r4's zonal slope of the equatorial thermocline, meridional and vertical currents, and strength of westward winds.

At each site the ECCOv4r4 core speed temporal variability was considerably less than ADCP. Ratios of ECCOv4r4 to ADCP variances at 165°E, 170°W, 140°W, and 110°W were 0.42, 0.65, 0.31, and 0.31, respectively. The rms difference between ECCOv4r4 and ADCP core speeds increased monotonically along the equator from 29.5 cm s^{-1} at 165°E to 58.9 cm s^{-1} at 110°W. The rms difference between ECCOv4r4 and ADCP zonal currents decreased above and below the depth of the core speed; e.g., at 140°W, the rms differences were 44.2 cm s^{-1} at 75 m (Fig. 1a) and 54.6 cm s^{-1} at the 105-m depth of the core speed (Fig. 3c). The large longitudinal variations between differences in ECCOv4r4 and ADCP variances and in rms differences substantiate a requirement for EUC comparative studies to encompass a range of longitudes.

The ECCOv4r4 and ADCP 1-h-averaged core speeds were generally well correlated, with correlation coefficients of 0.74, 0.81, 0.79, and 0.48, respectively, at 165°E, 170°W, 140°W, and 110°W. Not surprisingly, correlation coefficients with monthly-mean core speeds were higher: 0.84, 0.88, 0.87, and 0.53 at 165°E, 170°W, 140°W, and 110°W, respectively. We are surprised that ECCOv4r4 and ADCP core speeds at 110°W were relatively uncorrelated compared to the other three sites, and cannot explain the result.

Orthogonal regression analysis of monthly-mean EUC core speeds provided a formulation for ECCOv4r4 core speeds to be a proxy or stand-in for true or ADCP core speeds. A least squares line was defined by

$$\text{ADCP} = a\ \text{ECCOv4r4} + b, \tag{1}$$

where a is line slope and b is intercept of the line on the ordinate axis. Line slopes were 1.42, 1.12, 1.89, and 2.52 at 165°E, 170°W, 140°W, and 110°W, respectively; all values were statistically significant with 95% confidence. Intercept values were 16.81, 23.80, −5.21, and −15.86 cm s^{-1} at 165°E, 170°W, 140°W, and 110°W, respectively. The 95% uncertainty range of an ADCP core speed predicted from Eq. (1) is ±2 times the standard error (SE) of the regression line slope. Standard errors were 8.2, 10.7, 17.0, and 35.9 cm s^{-1} at 165°E, 170°W, 140°W, and 110°W, respectively. At 110°W, the simple regression model [Eq. (1)] would be inadequate to calculate monthly-mean ADCP core speeds from ECCOv4r4 core speeds because the

correlation coefficient between ECCOv4r4 and ADCP core speeds was low (0.53) and standard error was high. At 140°W, Eq. (1) seemed to be an appropriate statistical model to estimate ADCP core speeds from ECCOver4 data since the standard error was not large and correlation coefficient was high (0.87). At 165°E and 170°W, Eq. (1) represented a satisfactory model to estimate ADCP core speeds from ECCOv4r4 currents as correlation coefficients were above 0.83 and standard errors were less than 11 cm s^{-1}.

d. EUC transport

Knox and Halpern (1982) reported the transport per unit width (TPUW) at 152°W or 110°W was strongly linearly correlated with total EUC transport. The EUC TPUW at the equator is considered a proxy for EUC transport and is equal to $\int u(z)dz$, where $u(z)$ is the eastward current at depth z. Because an ADCP did not adequately record currents above 35 m, the upper depth of the transition between the SEC and EUC was not always known, especially at 110°W (Fig. 2d). To estimate TPUW we arbitrarily chose the depths of 20 cm s^{-1} to be the depths of the upper and lower limits of the integration; i.e., $\int udz$ was integrated vertically for $u(z)$ greater than 20 cm s^{-1}. This procedure enabled a similar vertical portion of the TPUW to be evaluated at each site, which provided an opportunity to estimate longitudinal variations of TPUW. At 165°E, 170° and 140°W, the upper and lower 20 cm s^{-1} isotachs were generally captured by ECCOv4r4 solutions and ADCP measurements (Figs. 2a–c) within the depth interval chosen at each site (section 2a). This situation did not occur as often at 110°W (Fig. 2d) where the upper depth of the 20 cm s^{-1} isotach was considerably shallower than at the other sites because the depth of the EUC shoaled from 165°E to 110°W. When the monthly-mean eastward current at the uppermost depth was higher than 20 cm s^{-1}, then the value of the zonal current at the uppermost depth was used to compute TPUW. This method yielded a TPUW that would be less than the value had the vertical profile of zonal current extended above the uppermost depth and captured the depth of the upper 20 cm s^{-1} isotach. At 110°W, this situation was prevalent with ADCP measurements compared to ECCOv4r4 currents (Fig. 2d), indicating a lower bound for the difference between ECCOv4r4 and ADCP TPUWs.

Monthly-mean ECCOv4r4 and ADCP TPUWs were strongly correlated with correlation coefficients at 165°E, 170°W, 140°W, and 110°W equal to 0.74, 0.91, 0.93, and 0.71, respectively. At each site, these values were larger than correlation coefficients between ECCOv4r4 and ADCP EUC core speeds, which was expected because a TPUW represents a vertically averaged current. At the four sites, a monthly-mean ECCOv4r4 TPUW was less than ADCP data, except on 5 of 499 occasions (or 1%). The ECCOv4r4 four-site-averaged TPUW was 46.6 m^2 s^{-1} or 51% smaller than ADCP measurements. Using Eq. (1) for monthly-mean TPUW, line slopes were 1.12, 1.17, 1.43, and 2.09 at 165°E, 170°W, 140°W, and 110°W, respectively; all values were statistically significant with 95% confidence. Intercepts were 24.59, 27.45, 29.65, and 25.65 m^2 s^{-1} at 165°E, 170°W, 140°W, and 110°W, respectively. Standard errors of the regression line slope at 165°E, 170°W, 140°W, and 110°W were 14.7, 14.7, 15.2, and 27.0 m^2 s^{-1}, respectively. At 170° and 140°W, the high correlations and low standard errors between ECCOv4r4 and ADCP TPUWs justified using Eq. (1) to linearly link ADCP TPUWs with ECCOv4r4 TPUWs. At 165°E, the low standard error indicated that Eq. (1) would be marginally usable since the square of the correlation coefficient indicated that only 55% of the variances were linearly related. At 110°W, Eq. (1) would be a weak model to estimate an ADCP TPUW because the correlation was low and the high standard error was nearly 2 times greater compared to those at the other sites.

As the EUC moved eastward from 165°E to 170°W, record-length ECCOv4r4 and ADCP TPUWs increased 1.6 and 2.0 m^2 s^{-1} per degree longitude, respectively, which was a difference of 20%. From 170° to 140°W, the ECCOv4r4 EUC increased its mass per unit width by 0.4 m^2 s^{-1} per degree longitude, which was 66% smaller than that recorded by ADCPs. From 140° to 110°W, both ECCOv4r4 and ADCP TPUWs showed a similar loss, although at 110°W the ECCOv4r4 TPUW strength was about 65% smaller than that determined with ADCP. Differences in ECCOv4r4 and ADCP EUC TPUWs would influence their respective representations of the amounts of meridional and upward inflows and outflows to the EUC.

Differences between monthly-mean ECCOv4r4 and ADCP TPUWs varied between sites. Mean ECCOv4r4 TPUWs at 140° and 110°W were smaller by 60.3 and 62.2 m^2 s^{-1}, respectively, compared to ADCP TPUWs. Standard deviations of monthly-mean ECCOv4r4 and ADCP differences were 16.9 and 22.3 m^2 s^{-1} at 140° and 110°W, respectively. However, a short-period notable exception appeared in the eastern equatorial Pacific in December 1997 at 140°W and in December 1997–January 1998 at 110°W when monthly-mean ECCOv4r4 and ADCP TPUWs were each about 0 m^2 s^{-1} to within 2 m^2 s^{-1}. These equivalences happened only at the aforementioned times in 10–14-yr times series of monthly-mean ECCOv4r4 and ADCP TPUWs. Considering the substantial differences between ECCOv4r4 and ADCP TPUWs over the entire record, it is puzzling that both ECCOv4r4 solutions and ADCP measurements indicated the absence of the EUC. Occurrences of virtual equality of monthly-mean ECCOv4r4 and ADCP TPUWs at 140° and 110°W were statistical outliers with about 99% certainty; i.e., their values were equal to the mean ECCOv4r4-minus-ADCP TPUW plus approximately 3 times the standard deviation. Without an extensive investigation of ECCOv4r4, which is beyond the scope of this work, we cannot speculate how ECCOv4r4 TPUWs would produce the disappearance of the EUC in the one-in-a-century El Niño event of May 1997–May 1998 (https://origin.cpc.ncep.noaa.gov/products/analysis_monitoring/ensostuff/ONI_v5.php). Initial observations of the disappearance of the EUC were recorded in the central (Firing et al. 1983) and eastern Pacific (Halpern 1987a) in the previous one-in-a-century El Niño event of April 1982–June 1983.

e. Temporal variations

The equatorial ocean hosts a variety of wave motions (Philander 1990). Fluctuations of surface wind stress, upwelling,

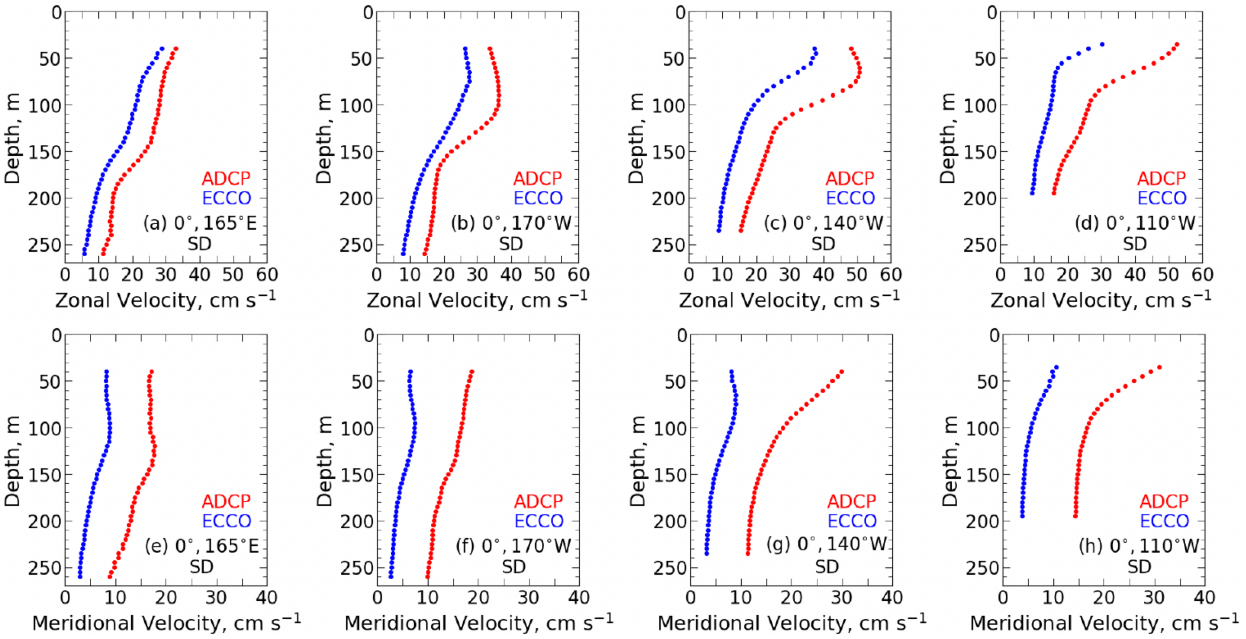

FIG. 4. Vertical profiles of record-length standard deviations of 1-h-averaged (top) zonal and (bottom) meridional currents at (a),(e) 165°E, (b),(f) 170°W, (c),(g) 140°W, and (d),(h) 110°W along the equator. Blue and red curves represent ECCOv4r4 and ADCP, respectively.

thermocline depth, and EUC transport yield a plethora of waves, including inertia–gravity, Kelvin, and Rossby waves, tropical instability waves, and seasonal to interannual adjustments of the EUC.

ECCOv4r4 currents did not adequately capture time variations measured by ADCP instruments. At all depths at each site, ECCOv4r4 SDs were substantially less than ADCP SDs for both zonal and meridional currents (Fig. 4). The maximum difference between ECCOv4r4 and ADCP SDs was 44.9 cm s^{-1} in the zonal current at 50-m depth at 110°W.

Spectral analysis disentangles a times series into frequency components. We used the Python NumPy library to compute periodogram ordinates from a time series in which the mean value has been removed. The NumPy software requires a time series with evenly spaced data. The small number of ADCP gaps (described in section 2a) were filled with linear interpolation. ECCOv4r4 data gaps, which had been created to synchronize gaps in ADCP time series to harmonize analyses (section 2a), were also filled by linear interpolation. To satisfy Parseval's theorem that the sum of all periodogram ordinates times the frequency band associated with each periodogram ordinate was equal to the total variance, each periodogram ordinate was normalized by

$$\frac{\sigma^2}{\sum_{i=1}^{N/2} P_i \Delta f},$$

where σ^2 is the record-length variance, N is the total number of 1-h-averaged zonal or meridional current measurements, i is the harmonic number of the periodogram, P_i is the ith harmonic periodogram ordinate density, $\Delta f = 1/(N\Delta t)$ is the frequency interval associated with each P_i, and Δt is the 1-h uniform time interval between successive data values of the continuous time series. Each P_i has 2 degrees of freedom. Confidence intervals at the 95% level were determined from the chi-square distribution for each spectral frequency band where the number of degrees of freedom was equal to the number of periodogram ordinates summed in the frequency band multiplied by 2.

We examined ECCOv4r4 and ADCP meridional and zonal current spectra at only two depths, 75 and 105 m, and a single site, 140°W (Fig. 5). We chose these depths because Fig. 1 showed time series of meridional and zonal currents at 75 m and Fig. 3c displayed the zonal current time series at 105 m. We chose 140°W because the strength of the EUC was near maximum at this longitude (Johnson et al. 2002; Halpern et al. 2015; Karnauskas et al. 2020), although it remains a mystery why this is so. Limited resources prevented a comprehensive mapping of ECCOv4r4 and ADCP spectral similarities and differences at all sites and depths. Our results will indicate further studies are warranted.

At the annual cycle [1.14×10^{-4} cycles per hour (cph)], ECCOv4r4 and ADCP zonal and meridional current spectral peaks at 75 and 105 m (Figs. 5a,c) were not statistically significant at the 95% confidence level. However, the annual cycles of ECCOv4r4 and ADCP zonal currents were evident in the time series (Fig. 1).

For frequencies above 2×10^{-2} cph, spectral differences between ECCOv4r4 and ADCP zonal and meridional currents were significant at the 95% confidence level, reaching maximum values at the Nyquist frequency (Fig. 5). The high-

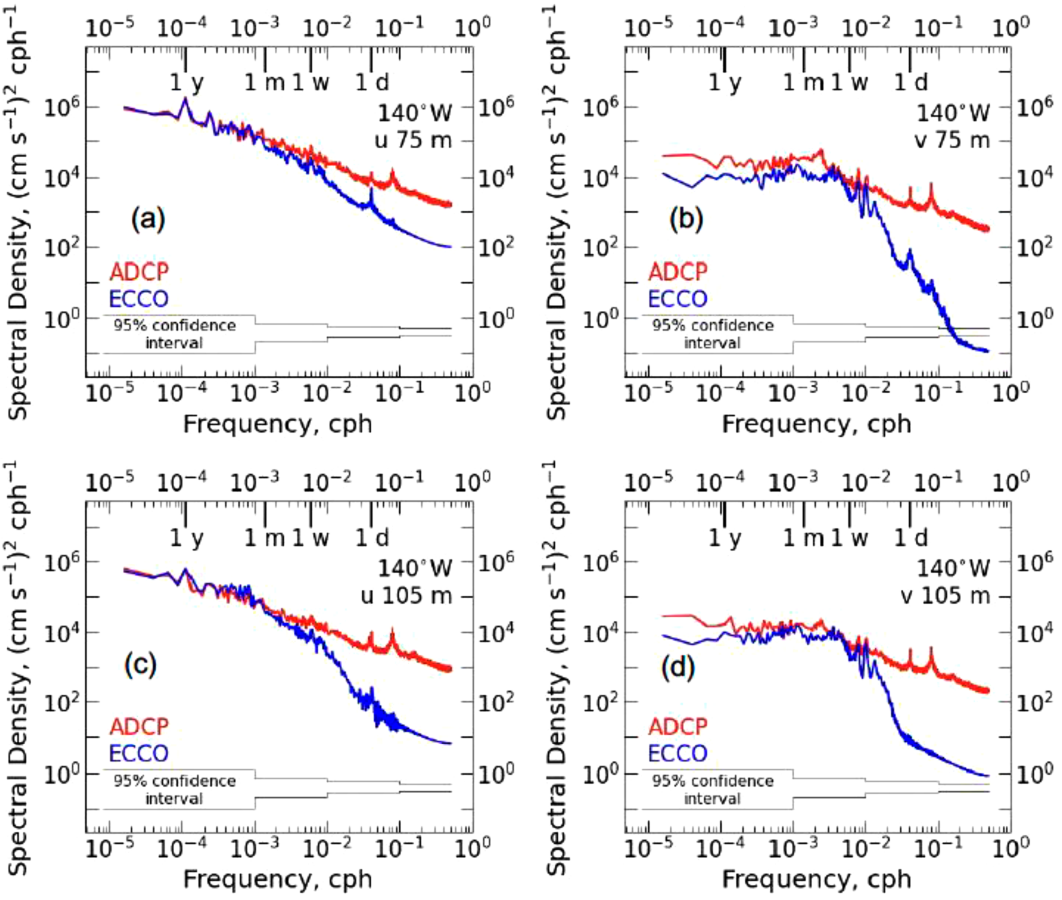

FIG. 5. Spectra of (a),(c) zonal currents and (b),(d) meridional currents at (a),(b) 75-m depth and (c),(d) 105 m at 140°W. Blue and red curves represent ECCOv4r4 and ADCP, respectively. The 95% confidence limits are displayed in each panel. Inside each panel, the symbols "y," "m," "w," and "d" represent "year," "month," "week," and "day."

frequency smaller-amplitude motions associated with ECCOv4r4 currents compared to ADCP measurements were visible in the time series (Fig. 1). Smallest and largest such differences occurred at 75 m, where differences were factors of 15 (Fig. 5a) and 5000 (Fig. 5b), respectively.

We expected ADCP measurements at 75 and 105 m at 140°W to contain semidiurnal- and diurnal-period tidal currents with meridional and zonal amplitudes statistically significant with 95% confidence (Fig. 5) (Weisberg et al. 1987; Halpern et al. 1988). However, we did not expect ECCOv4r4 solutions at 75 m to have diurnal-period tidal currents significant with 95% confidence with rms meridional and zonal current amplitudes of about 0.8 (Fig. 5b) and 4.8 (Fig. 5a) cm s^{-1}, respectively. The zonal current diurnal-period amplitude produced by ECCOv4r4 compared to ADCP (Fig. 5a) was also unpredicted; also, its larger amplitude was confusing. At the semidiurnal frequency, the absence of spectral peaks statistically significant with 95% confidence (Fig. 5) was expected. The MITgcm in ECCOv4r4 did not include a mechanism to generate tidal currents. Tidal currents could have been generated by atmospheric surface forcing, such as air pressure and wind stress. However, the ECCOv4r4 formulation removed the spectral content from the pressure field at 9 tidal frequencies (ECCO Consortium et al. 2021). Along the equator, the diurnal-period surface wind oscillation had a 30 cm s^{-1} rms amplitude (Halpern 1988) and it is tempting to suppose that surface winds generated diurnal-period internal wave motion at 75 m. Interestingly, the ECCOv4r4 data assimilation scheme was not a likely source of diurnal-period currents because in situ salinity and temperature profiles were averaged over 1 day.

f. Gradient Richardson number

A gradient Richardson number (Ri) less than 1/4 represents the tendency for sheared flow in a density-stratified fluid to develop vertical mixing (Howard 1961; Miles 1961). Galperin et al. (2007) suggested that turbulence survives for Ri below 1.

We report on estimates of 1-h Ri between the depth of the core speed and upper and lower depths in the EUC where the zonal current at depth z was equal to 20 cm s^{-1}. The Ri is defined by

$$\mathrm{Ri} = N(z)^2/[(du/dz)^2 + (dv/dz)^2],$$

where $N(z)$ is the Brunt–Väisälä frequency, $v(z)$ is the meridional current component, and du/dz and dv/dz are the zonal

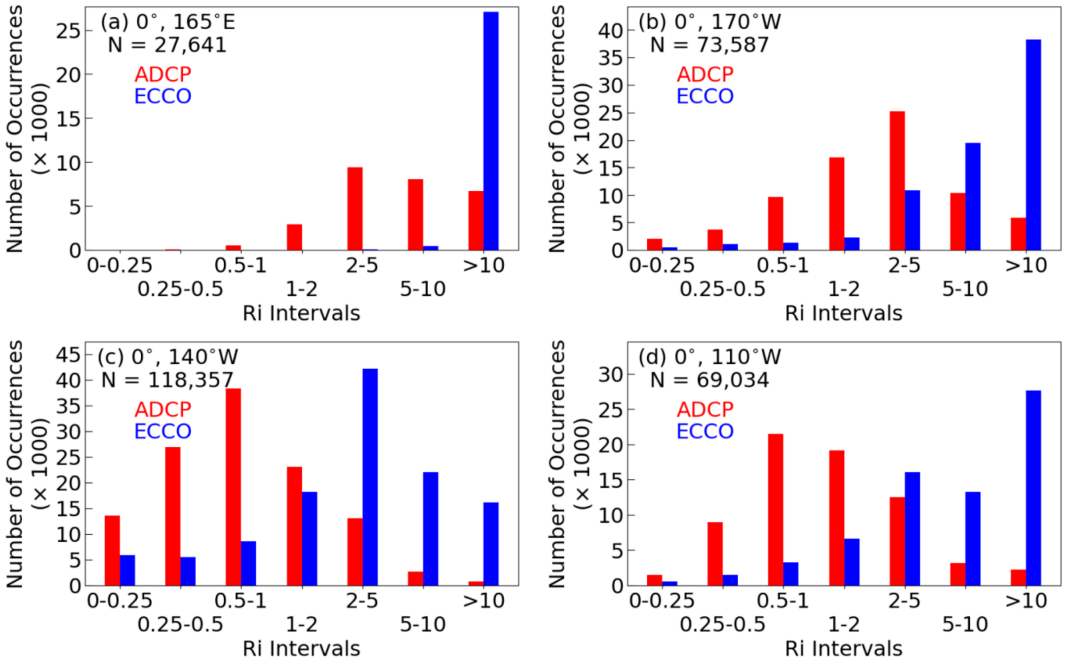

FIG. 6. Histograms of number of occurrences of ECCOv4r4 (blue) and ADCP (red) 1-h-averaged Ri with nonuniform Ri intervals in the upper layer between the depth of the core speed and the upper depth where the zonal current was 20 cm s^{-1}: (a) 165°E, (b) 170°W, (c) 140°W, and (d) 110°W. N is the total number of Ri values.

and meridional components, respectively, of the vertical shear or vertical gradient of velocity. At the sea surface, $z = 0$ and is positive upward. We define $N(z)$ by

$$N(z) = [-g/\rho(z)][d\rho(z)/dz]^{1/2},$$

where $\rho(z)$ is the density at depth z, $d\rho/dz$ is the vertical gradient of density, and g is the acceleration due to gravity (9.8 m s^{-2}). Climatological mean-monthly values of density were obtained from the *World Ocean Atlas 2018* (*WOA*) (https://www.ncei.noaa.gov/access/world-ocean-atlas-2018/) using 1995–2004 mean values. *WOA* horizontal grid dimension of the density dataset was 1° latitude × 1° longitude and we averaged densities in each of four cells adjacent to each location. Because *WOA* did not have density data at all ADCP depths, density values were linearly interpolated from the nearest depths. The same density values were used with ECCOv4r4 and ADCP currents. Although ECCOv4r4 and ADCP values of Ri were evaluated with identical vertical distributions of density, the Ri provides a vertical-mixing context to interpret differences between ECCOv4r4 and ADCP vertical profiles of meridional and zonal currents.

All record-length ECCOv4r4 mean Ri values were greater than ADCP values. This was not surprising because ECCOv4r4 core speeds were less than those computed with ADCP data (Figs. 2 and 3). Consequently, ECCOv4r4 vertical shears of the zonal current between the depth of the core speed and upper and lower depths where $u(z) = 20$ cm s^{-1} were smaller than those computed with ADCP measurements. Vertical shears of meridional currents were much less than those of zonal currents (Fig. 2). In the upper layer, the four-site-averaged time-mean ECCOv4r4 Ri (=70.1) was 11.5 times higher than the ADCP value. In the lower layer, this ratio was 15.8. The lower layer had far fewer occurrences of Ri < 1/4 compared to the upper layer. At 140°W, ECCOv4r4 and ADCP had the largest numbers of 1-h Ri < 1/4 compared to other sites, especially in the upper layer (Fig. 6). In the upper layer at each site, the number of times that 1-h-averaged Ri were less than 1/4, between 1/4 and 1/2, and between 1/2 and 1 were considerably less for ECCOv4r4 than ADCP (Fig. 6). For example, at 140°W, the number of ECCOv4r4 Ri occurrences in the upper layer for Ri below 1/4, between 1/4 and 1/2, and between 1/2 and 1 were about 65%, 80%, and 85% smaller than ADCP Ri occurrences, respectively. Additional studies of the ECCOv4r4 parameterization of upper-ocean vertical mixing along the equator are warranted, especially at 140°W where observational ocean-mixing campaigns occurred (e.g., Gregg 2021).

4. Summary

In comparison with ADCP measurements, ECCOv4r4 produced a highly realistic time-averaged and variable EUC over time scales of hours to years at widely spaced longitudes; however, ECCOv4r4 amplitudes were generally too small. Results of comparisons of 10–14-yr ECCOv4r4 and ADCP currents at 165°E, 170°W, 140°W, and 110°W in the Pacific EUC included the following:

1) Correspondence between ECCOv4r4 and ADCP depths of the EUC core speed was excellent (section 3b).
2) ECCOv4r4 vertical- and longitudinal-averaged mean zonal current was about 50% smaller than ADCP (section 3b).

3) ECCOv4r4 longitudinal-averaged mean EUC core speed was about 50% smaller than ADCP (section 3c).
4) Longitudinal-averaged ECCOv4r4 core speed variance was about 40% smaller than ADCP (section 3c).
5) Linear regression analysis indicated that ECCOv4r4 core speeds at 165°E, 170°W, and 140°W could be a proxy of ADCP core speeds (section 3c).
6) Longitudinal-averaged ECCOv4r4 TPUW was about 50% smaller than ADCP (section 3d).
7) Linear regression analysis indicated that ECCOv4r4 TPUWs at 170° and 140°W could be a proxy of ADCP TPUWs (section 3d).
8) ECCOv4r4 TPUW increased about 66% less than ADCP from 170° to 140°W (section 3d).
9) We are perplexed why at 110°W correlation coefficients between ECCOv4r4 and ADCP core speeds and TPUWs were substantially lower and the linear regression model was much weaker compared to the other sites (sections 3c and 3d). Perhaps this characteristic of the comparative study is revealing the incapability of the ECCOv4r4 formulations of mixing and upwelling where the EUC was closest to the sea surface compared to the other sites. The depth of the EUC core speed increased westward, increasing to a depth more than twice as deep at 165°E (section 3c).
10) ECCOv4r4 meridional and zonal current standard deviations were considerably less than ADCP's at all depths and sites (section 3e).
11) The appearance of ECCOv4r4 diurnal-period zonal current oscillations was unexpected (section 3e).
12) ECCOv4r4 vertical shear of zonal currents was smaller than ADCP, producing ECCOv4r4 upper-ocean Ri much larger than ADCP and number of occurrences of Ri $< 1/4$ much less than ADCP (section 3f).

5. Concluding remarks

Currents at the equator are particularly challenging for OGCMs to simulate because of the absence of geostrophy. Our findings demonstrated that the ECCOv4r4 representation of EUC horizontal velocities would not be an appropriate proxy for moored in situ current measurements in the EUC. However, we show that ECCOv4r4 and ADCP currents have a strong correlated linear relationship. Thus, ECCOv4r4 currents could provide valid representations of the EUC when its output is supplemented by a simple linear regression model. This method satisfies our primary motivation whether ECCOv4r4 currents would be a suitable proxy for in situ current measurements in the EUC. To improve ECCOv4r4 currents, additional studies are warranted to investigate the impacts of (i) strength of surface winds, (ii) intensity of upper-ocean mixing parameterization, and (iii) reduction in latitudinal grid dimension. The next version of ECCOv4r4, which is called ECCO version 5, and expected for release in 2024, will have a nominal 1/3° grid spacing throughout 10°S–10°N. At the equator, the ECCOv5's 33-km north–south grid dimension will be advantageous (Hoteit et al. 2008) because it will be 22% smaller than in ECCOv4r4, although not as advantageous as a smaller grid size such as 0.25° (Karnauskas et al. 2020). Verdy et al. (2017) demonstrated that a 33-km spacing of the north–south grid of an ECCOv4r4-type of model–data system may be too large to capture the intensity of the EUC.

The Pacific EUC currents produced by ECCOv4r4 and other OGCM–data systems are rarely validated beyond a cursory examination of the mean vertical profile for a qualitative assessment that an EUC is produced (section 1). Our results indicated increased testing of OGCM-generated currents with in situ measurements is warranted and, perhaps, will introduce surprising performances. Differences will be a gold mine for discoveries to improve OCGM–data systems.

Acknowledgments. We gratefully acknowledge NASA and NOAA for sustained operations of ECCO and GTMBA, respectively. We thank Ian Fenty (JPL), Ichiro Fukumori (JPL), Dai McClurg (PMEL), and Ou Wang (JPL) for help with ECCOv4r4 and ADCP datasets. We thank Bruce Cornuelle (SIO), Yassir Eddebbar (SIO), Noel Gutierrez-Brizuela (SIO), and Ichiro Fukumori (JPL) for discussions on an early version of the manuscript. We thank three anonymous reviewers for comments to improve the manuscript. P.H. was supported in part by NOAA OAR/CPO Grant NA21OAR4310255. T.A.S. was supported in part by a JPL/Caltech subcontract of the ECCO consortium. This has been a private undertaking for D.H. and M.K.L. D.H. is affiliated with JPL in a management activity which is totally independent of the work described herein.

Data availability statement. ECCOv4r4 data are available at Smith (2021). ADCP data are available at the Global Tropical Moored Buoy Array (GTMBA) project (https://www.pmel.noaa.gov/gtmba/pmel-theme/pacific-ocean-tao).

REFERENCES

Bjerknes, J., 1969: Atmospheric teleconnections from the equatorial Pacific. *Mon. Wea. Rev.*, **97**, 163–172, https://doi.org/10.1175/1520-0493(1969)097<0163:ATFTEP>2.3.CO;2.

Callahan, C. W., and J. S. Mankin, 2023: Persistent effect of El Niño on global economic growth. *Science*, **380**, 1064–1069, https://doi.org/10.1126/science.adf2983.

Colin, C., C. Henin, P. Hisard, and C. Oudot, 1971: Le courant de Cromwell dans le Pacifique central en février. *Cah. ORSTOM Ser. Oceanogr.*, **9**, 167–186.

Cromwell, T., R. B. Montgomery, and E. D. Stroup, 1954: Equatorial Undercurrent in the Pacific revealed by new methods. *Science*, **119**, 648–649, https://doi.org/10.1126/science.119.3097.648.

ECCO Consortium, I. Fukumori, O. Wang, I. Fenty, G. Forget, P. Heimbach, and R. M. Ponte, 2021: Synopsis of the ECCO Central Production global ocean and sea-ice state estimate (version 4 release 4). Zenodo, https://doi.org/10.5281/zenodo.4533349.

Firing, E., R. Lukas, J. Sadler, and K. Wyrtki, 1983: Equatorial Undercurrent disappears during 1982-83 El Niño. *Science*, **222**, 1121–1123, https://doi.org/10.1126/science.222.4628.1121.

Forget, G., J.-M. Campin, P. Heimbach, C. N. Hill, R. M. Ponte, and C. Wunsch, 2015: ECCO version 4: An integrated framework for non-linear inverse modeling and global state

estimation. *Geosci. Model Dev.*, **8**, 3071–3104, https://doi.org/10.5194/gmd-8-3071-2015.

Fukumori, I., 2006: What is data assimilation really solving and how is the calculation really done? *Ocean Weather Forecasting*, E. P. Chassignet and J. Verron, Eds., Springer, 317–342.

Galperin, B., S. Sukoriansky, and P. S. Anderson, 2007: On the critical Richardson number in stably stratified turbulence. *Atmos. Sci. Lett.*, **8**, 65–69, https://doi.org/10.1002/asl.153.

Gill, A. E., 1975: Models of equatorial currents. *Numerical Models of Ocean Circulation*, National Academy of Science, 181–203.

Gregg, M. C., 2021: *Ocean Mixing*. Cambridge University Press, 378 pp.

Halpern, D., 1987a: Observations of annual and El Niño thermal and flow variations along the equator at 0°, 110°W and 0°, 95°W during 1980–1985. *J. Geophys. Res.*, **92**, 8197–8212, https://doi.org/10.1029/JC092iC08p08197.

——, 1987b: Comparison of upper ocean VACM and VMCM observations in the equatorial Pacific. *J. Atmos. Oceanic Technol.*, **4**, 84–93, https://doi.org/10.1175/1520-0426(1987)004<0084:COUOVA>2.0.CO;2.

——, 1988: Moored surface wind observations at four sites along the Pacific equator between 140°W and 95°W. *J. Climate*, **1**, 1251–1260, https://doi.org/10.1175/1520-0442(1988)001<1251:MSWOAF>2.0.CO;2.

——, 2021: Origin of sustained measurements of surface wind and upper-ocean current and temperature on the Pacific equator: EQUA project. *Bull. Amer. Meteor. Soc.*, **102**, E1862–E1877, https://doi.org/10.1175/BAMS-D-20-0314.1.

——, and H. P. Freitag, 1987: Vertical motion in the upper ocean of the equatorial eastern Pacific. *Oceanol. Acta*, **6**, 19–26.

——, R. A. Knox, and D. S. Luther, 1988: Observations of 20-day period meridional current oscillations in the upper ocean along the Pacific equator. *J. Phys. Oceanogr.*, **18**, 1514–1534, https://doi.org/10.1175/1520-0485(1988)018<1514:OODPMC>2.0.CO;2.

——, D. Menemenlis, and X. Wang, 2015: Impact of data assimilation on ECCO2 Equatorial Undercurrent and North Equatorial Countercurrent in the Pacific Ocean. *J. Atmos. Oceanic Technol.*, **32**, 131–143, https://doi.org/10.1175/JTECH-D-14-00025.1.

——, M. Le, and T. Smith, 2022: How accurate are ECCOv4r4 estimates of the Pacific Equatorial Undercurrent? *Ocean Sciences Meeting 2022*, Online, OSM, AI09, https://osm2022.secure-platform.com/a/gallery/rounds/3/details/5285.

Hoteit, I., B. Cornuelle, V. Thierry, and D. Stammer, 2008: Impact of resolution and optimized ECCO forcing on simulations of the tropical Pacific. *J. Atmos. Oceanic Technol.*, **25**, 131–147, https://doi.org/10.1175/2007JTECHO528.1.

Howard, L. N., 1961: Note on a paper by John W. Miles. *J. Fluid Mech.*, **10**, 509–512, https://doi.org/10.1017/S0022112061000317.

Janjić, T., and Coauthors, 2017: On the representation error in data assimilation. *Quart. J. Roy. Meteor. Soc.*, **144**, 1257–1278, https://doi.org/10.1002/qj.3130.

Johnson, G. C., B. M. Sloyan, W. S. Kessler, and K. E. McTaggart, 2002: Direct measurements of upper ocean currents and water properties across the tropical Pacific during the 1990s. *Prog. Oceanogr.*, **52**, 31–61, https://doi.org/10.1016/S0079-6611(02)00021-6.

Joshi, M., 2023: El Niño could push global warming past 1.5 C—But what is it and how does it affect the weather in Europe? Phys.org., https://phys.org/news/2023-06-el-nio-global-cbut-affect.html.

Karnauskas, K. B., J. Jakoboski, T. M. S. Johnston, W. B. Owens, D. L. Rudnick, and R. E. Todd, 2020: The Pacific Equatorial Undercurrent in three generations of global climate models and glider observations. *J. Geophys. Res. Oceans*, **125**, e2020JC016609, https://doi.org/10.1029/2020JC016609.

Kessler, W. S., and Coauthors, 2021: Final report of TPOS 2020. GOOS Rep. GOOS-268, 83 pp., https://tropicalpacific.org/tpos2020-project-archive/reports/.

Knox, R. A., and D. Halpern, 1982: Long range Kelvin wave propagation of transport variations in Pacific Ocean equatorial currents. *J. Mar. Res.*, **40**, 329–339.

Marshall, J., C. Hill, L. Perelman, and A. Adcroft, 1997a: Hydrostatic, quasi-hydro-static, and nonhydrostatic ocean modeling. *J. Geophys. Res.*, **102**, 5733–5752, https://doi.org/10.1029/96JC02776.

——, A. Adcroft, C. Hill, L. Perelman, and C. Heisey, 1997b: A finite-volume incompressible Navier Stokes model for studies of the ocean on parallel computers. *J. Geophys. Res.*, **102**, 5753–5766, https://doi.org/10.1029/96JC02775.

Miles, J. W., 1961: On the stability of heterogeneous shear flows. *J. Fluid Mech.*, **10**, 496–508, https://doi.org/10.1017/S0022112061000305.

Ou, W., I. Fukumori, and I. Fenty, 2020: ECCO version 4 release 4 user guide. NASA ECCO, https://www.ecco-group.org/user-guide-v4r4.htm.

Philander, S. G. H., 1973: Equatorial Undercurrent: Measurements and theories. *Rev. Geophys.*, **11**, 513–570, https://doi.org/10.1029/RG011i003p00513.

——, 1990: *El Niño, La Niña, and the Southern Oscillation*. Academic Press, 293 pp.

——, and A. D. Siegel, 1985: Simulation of El Niño of 1982–83. *Coupled Ocean-Atmosphere Models*, J. C. L. Nihoul, Ed., Elsevier, 517–541.

Plimpton, P. E., H. P. Freitag, and M. J. McPhaden, 2004: Processing of subsurface ADCP data in the equatorial Pacific. NOAA Tech. Memo. OAR PMEL-125, 45 pp., https://tao.ndbc.noaa.gov/proj_overview/pubs/PDF/plimpton_adcp.pdf.

Plumer, B., 2014: Scientists were expecting a big El Niño. So where did it go? *Vox*, 8 November, https://www.vox.com/2014/11/8/7177709/el-nino-2014-forecast-weakening.

Rowntree, P. R., 1972: The influence of tropical east Pacific Ocean temperature on the atmosphere. *Quart. J. Roy. Meteor. Soc.*, **98**, 290–321, https://doi.org/10.1002/qj.49709841605.

Smith, T., 2021: ECCOv4r4 tropical Pacific velocity fields. Figshare, accessed 9 January 2021, https://doi.org/10.6084/m9.figshare.16557387.v1.

Stammer, D., and Coauthors, 2002: Global ocean circulation during 1992–1997 estimated from ocean observations and a general circulation model. *J. Geophys. Res.*, **107**, 3118, https://doi.org/10.1029/2001JC000888.

——, M. Balmaseda, P. Heimbach, A. Köhl, and A. Weaver, 2016: Ocean data assimilation in support of climate applications: Status and perspectives. *Annu. Rev. Mar. Sci.*, **8**, 491–518, https://doi.org/10.1146/annurev-marine-122414-034113.

Sverdrup, H. U., 1947: Wind-driven currents in a baroclinic ocean with application to the equatorial currents in the eastern Pacific. *Proc. Natl. Acad. Sci. USA*, **33**, 318–326, https://doi.org/10.1073/pnas.33.11.318.

Teledyne RD Instruments, 2011: Acoustic Doppler current profiler principles of operation: A practical primer. Teledyne Tech. Rep. P/N 951-6069-00, 62 pp., https://www.comm-tec.com/Docs/Manuali/RDI/BBPRIME.pdf.

Verdy, A., B. Cornuelle, M. R. Mazloff, and D. L. Rudnick, 2017: Estimation of the tropical Pacific Ocean state 2010–2013. *J. Atmos. Oceanic Technol.*, **34**, 1501–1517, https://doi.org/10.1175/JTECH-D-16-0223.1.

Weisberg, R. H., D. Halpern, T. Y. Tang, and S. M. Hwang, 1987: M_2 tidal currents in the eastern equatorial Pacific Ocean. *J. Geophys. Res.*, **92**, 3821–3826, https://doi.org/10.1029/JC092iC04p03821.

Weller, R. A., and R. E. Davis, 1980: A vector measuring current meter. *Deep-Sea Res.*, **27A**, 565–581, https://doi.org/10.1016/0198-0149(80)90041-2.

World Climate Research Program, 1985: Scientific plan for the Tropical Oceans and Global Atmosphere program. WMO Tech. Doc. WMO/TD-64, 146 pp.

Wunsch, C., and P. Heimbach, 2013: Dynamically and kinematically consistent global ocean circulation and ice state estimates. *Ocean Circulation and Climate: A 21st Century Perspective*, G. Siedler et al., Eds., Elsevier, 553–579.